I.J. Information Technology and Computer Science, **2026, 1, 100-123**
Published Online on February 8, 2026 by MECS Press (http://www.mecs-press.org/)
DOI: 10.5815/ijitcs.2026.01.06

A Holistic Framework for Confidential Brain Tumor Diagnosis over IoMT: HWS-CSIWT and OBTSC-Net Integration

M. V. S. Ramprasad*
Department of Electronics and Communication Engineering, Koneru Lakshmaiah Education Foundation, Deemed to be University, Vaddeswaram, Andhra Pradesh, India
E-mail: molavantiramprasad@gmail.com
ORCID iD: https://orcid.org/0000-0002-3640-1637
*Corresponding author

Md. Zia Ur Rahman
Department of Electronics and Communication Engineering, Koneru Lakshmaiah Education Foundation, Deemed to be University, Vaddeswaram, Andhra Pradesh, India
E-mail: mdzr55@gmail.com
ORCID iD: https://orcid.org/0000-0002-4948-3870

Received: 28 August 2025; Revised: 13 November 2025; Accepted: 03 December 2025; Published: 08 February 2026

Abstract: The development of medical-imaging neurology diagnostics regarding brain tumor detection and classification via the Internet of Medical Things (IoMT) is important. This research proposes a comprehensive framework addressing user privacy concerns by embedding brain tumor information in a cover image through Hybrid Watermarking Steganography (HWS) using Compressive Sensing Integer Wavelet Transform (CSIWT). The watermarked images are securely transmitted over the IoMT, ensuring data integrity. An Inverse CSIWT-HWS system extracts the hidden brain tumor image for diagnosis. The proposed framework incorporates an Optimized Brain Tumor Segmentation and Classification Network (OBTSC-Net) to enhance diagnostic capabilities. This transfer learning model utilizes Attention Generative Adversarial Networks (AGAN) to segment brain tumor areas from the extracted images, Hybrid Greylag Goose Optimization Genetic Algorithm (HGGO-GA) for disease-specific feature extraction from segmented images, and Broad Learning System Neural Network (BLS-NN) for the accurate classification of benign and malignant brain tumors using BraTS-2020 and BraTS-2021 datasets, offering a reliable and secure tool for remote diagnosis. Finally, the proposed HWS-CSIWT method achieved an average Peak Signal-to-Noise Ratio (PSNR) improvement of 12.65% over existing state-of-the-art methods. The proposed AGAN method achieved an average segmentation accuracy (SACC) improvement of 5.63% over existing methods, and the proposed OBTSC-Net achieved an average classification accuracy (CACC) improvement of 2.82% over existing state-of-the-art methods, confirming its enhanced diagnostic capability in brain tumor classification.

Index Terms: Brain Tumor Detection, Internet of Medical Things, Data Security, Remote Diagnosis, Medical Information Transmission.

1. Introduction

Research on brain tumor classification remains central because neuro-oncologists need better diagnostic and treatment methodologies [1]. Brain tumors affect human health patterns regarding survival conditions and death rates. Globally, brain tumors exhibit diverse pathological and molecular features that necessitate complete comprehension to create effective, individualized therapeutic approaches [2].

The primary reason behind research into brain tumor classification is the complex and diverse nature of tumors. There are many diagnostic and treatment challenges: brain cancers present different histological types and many alterations in genetic mutations and clinical progression patterns [3]. Researchers work to discover complex molecular patterns and phenotypic modifications among brain tumor subtypes to create better-targeted treatments [4].

According to the literature, existing diagnostic approaches have several limitations, revealing the necessity for improved classification techniques [5]. The diagnostic power of radiological imaging combined with histopathological analysis fails to deliver complete awareness of relevant molecular changes [6]. Research into machine learning and artificial intelligence methodologies has emerged to enhance current diagnosis methods and discover new biomarkers for better classification outcomes [7].

Studies have focused on brain tumor classification research to provide essential benefits for treatment decision-making procedures and patient-outcome statistics [8]. Brain tumor classification leads medical staff to choose proper therapeutic options, such as surgical procedures, chemotherapy, and radiotherapy. Treatment decisions informed by cancer-specific qualities can maximize therapeutic results while reducing adverse effects and enhancing the overall standard of medical assistance for patients.

Recent brain tumor research has expanded its frontiers by merging several omics datasets, including genomics, transcriptomics, and proteomics data [9]. The complete analysis of tumor molecular patterns enables improved classification while enabling scientists to identify new treatment targets and develop personalized therapeutic methods [10]. Scientists explore neuro-oncological information because they understand that brain tumor molecular variations hold important knowledge. Mehnatkesh et al. designed an intelligent framework of deep residual learning that uses Magnetic Resonance Imaging (MRI) in brain tumor classification applications. The researchers' CACC methodology benefits from deep residual learning methods [11]. In [12], the researchers developed M3BTCNet as a multi-model brain tumor classification method that optimizes metaheuristic deep neural network features. The model uses deep neural networks coupled with metaheuristic optimization tools to enhance classification results. In [13], the authors introduced by Patil and Hamde described an upgraded local optimal-oriented pattern descriptor that employs steerable wavelet transform to classify tumors from MRI scans. The researchers identified steerable wavelet transform as a feature-extraction tool that improves classification precision.

Kishanrao and Jondhale [14] developed an enhanced grade-based MRI brain tumor classification method by implementing a Deer Hunting (DCNN-DH) framework into convolutional neural networks. The researchers implemented deep CNN with a hybrid framework to improve grade-based classification outcomes. In [15], the authors proposed MCNN as a multi-level CNN model that enables brain tumor classification within an Internet of Things (IoT) healthcare system. The researchers developed an IoT healthcare system for brain tumor classification by including various CNN levels for efficient performance. Rajeena and Sivakumar [16] developed a brain tumor classification system through image fusion integration with an EFPA-Support Vector Machine (SVM) classification model. A recently proposed method links image fusion approaches with EFPA-SVM classification processes to perform brain tumor identification effectively. Abd El-Wahab [17] developed BTC-fCNN, which stands for fast CNN for multiple brain tumor classification. The authors optimized their model for fast and efficient multiclass brain tumor recognition processes. Özkaraca et al. [18] established a brain MRI-based multiple brain tumor classification solution through dense CNN architecture. The researchers' model leverages a dense CNN for effective brain tumor classification.

Singh and Agarwal [19] developed an automatic brain tumor classification system for MRI based on advanced CNN architecture. The researchers designed a method to boost the effectiveness of CNNs in automated brain tumor classification. Muezzinoglu et al. [20] created PatchResNet, which conducts deep feature fusion and multiple patch division in a framework for brain tumor identification using MRI scans. Image patches, which are divided by their approach, enable deep features to combine for better CACC. Zhu et al. [21] developed a brain tumor classification system by implementing RBEBT, which combines ResNet architecture and BA-ELM algorithms for brain tumor classification. Asif et al. [22] demonstrated upgraded deep-learning techniques for brain tumor multi-classification through deep transfer learning strategies for improved classification outcomes in their system. Nanda et al. [23] combined SSO-RBNN for brain tumor classification and Saliency-K-means (SKM) segmentation features. The SKM segmentation technique joins forces with a self-organizing radial basis neural network for precise brain tumor classification. Kumar et al. [24] established a method for brain tumor classification and segmentation by implementing CNN as their methodology to both identify and segment brain tumors.

Haq et al. [25] developed the DCNNBT deep convolution neural network-based model for brain tumor classification. This deep CNN enables efficient brain tumor classification according to its design. Hossain et al. [26] described an efficient deep-learning-based microwave brain image network model that classifies brain tumors using reconstructed microwave brain images. The researchers developed a microwave imaging system for light and efficient brain tumor classification purposes. Shahin et al. [27] created a new multiclass brain tumor classifying system that utilizes unsupervised PCANet features as the base method. The researchers employed PCANet to extract features, which produces efficient results for multiclass brain tumor classification. Emam et al. [28] developed an optimized deep-learning system to classify brain tumors through their Hunger Games Search Algorithm (HGSA) optimization. This method achieves optimal deep-learning architecture performance, which improves brain tumor diagnosis capabilities. Shahin et al. [29] introduced MBTFCN, which is a modular, fully convolutional network that performs MRI brain tumor multi-classification. The system implements fully convolutional networks through its modular design for brain tumor multiclass classification. Athisayamani et al. [30] developed ResNet-152 as a Residual Deep CNN for extracting features, which they combined with feature-dimension optimization to achieve MRI brain tumor classification. Feature extraction and classification optimization form the basis of the analytical approach, which uses ResNet-152 for analysis.

Aloraini et al. [31] accomplished successful brain tumor classification through their integration of Transformer with Convolution components. A combination of Transformer with CNN enables efficient brain tumor classification. Lavanya et al. [32] developed a brain tumor classification system using an SVM classifier, which implemented seagull optimization. This algorithm serves as a hyperplane selection tool for SVM to achieve precise classification. Zulfiqar et al. [33] demonstrated how EfficientNet performs multiclass brain tumor identification from MR images. Brain tumor classification reaches high efficiency by implementing EfficientNet. Asiri et al [34] developed a fine-tuned CNN that combines ResNet50 and U-Net components, which served as the base for brain tumor detection and classification. Xiao et al. [35] accomplished brain tumor MRI classification through their implementation of contrastive learning that used dynamic weighting and jigsaw augmentation.

Geetha et al. [36] outlined a multi-level brain tumor classification system by integrating deep learning with Archimedes Sine Cosine Optimization (ASCO)-based processing of MRI scans. Khan et al. [37] demonstrated a brain tumor classification system by combining least square-SVM with multi-model texture features. Least squares SVM serves as part of the system, which integrates multi-model texture features for precise identification purposes. Cinar et al. [38] developed a new CNN system to classify brain tumors using MRI scans. The method leverages CNN for efficient brain tumor classification. In [39], the authors introduced a multi-level deep Generative Adversarial Network (GAN) for multi-level brain tumor classification from MRI scans. Ponnupilla Omana et al. [40] implemented Henry Gas Bird Swarm Optimization (HGBSO) algorithm-based deep learning for brain tumor MRI classification. The authors merged HGBSO with deep-learning techniques to achieve superior results in brain tumor classification.

1.1. Problem Statement

The survey examines existing methods that fall short in medical image diagnostic and transmission approaches regarding brain tumor evaluation. The lack of HWS systems that combine segmentation and classification capabilities creates major difficulties for medical data security throughout transmission procedures. There is a risk of exposure of patients' protected medical data because existing methods have documented security gaps. Productive utilization of existing diagnostic techniques is hampered because segmentation and classification require enhanced performance for improved accuracy and reliability.

1.2. Novelty of Work

The literature has revealed the need for the development of a dual watermarking-steganography system that identifies brain tumors, as this is a key research deficiency. Aligning these two technologies will signify a major revolution in medical image protection and analysis processes, resolving information security and diagnostic precision challenges. Such an innovative combination holds promise for protecting patient information while maintaining medical image authenticity to build trust in IoMT platforms. The creation of a CSIWT is an innovative approach to represent signals across medical images. This technique takes advantage of compressive sensing and integer wavelet transforms to provide a data compression method that reduces computational complexity and storage requirements in IoMT systems.

The third strength of the HGGO-GA method extends from its ability to merge distinct optimization approaches for selecting features in brain tumor classification tasks. The integration of Greylag Goose Optimization with Genetic Algorithms produces a strong approach to detecting important features hidden in high-dimensional medical image datasets. The newly integrated hybrid approach presents an opportunity to enhance brain tumor classification models, strengthening their generalization abilities and diagnostic precision.

Medical image analysis benefits significantly from the pioneering implementation of the Broad Learning System for brain tumor applications. This method highlights the potential to enhance tumor classification model performance through a broad learning network capacity to analyze complex heterogeneous medical data. The use of such broad learning techniques offers a new approach that benefits diagnosis accuracy and treatment-specific care for brain tumor patients, driving healthcare improvements and neuroimaging research.

1.3. Aim of Work

The main goal of this proposed research work concerns resolving significant brain tumor diagnostic issues by focusing primarily on secure and efficient IoMT-based medical data transfer operations. Advanced medical imaging today demands substantial privacy protection methods and data integrity safeguards, which are fundamental in the modern clinical environment. The work commences by focusing on data confidentiality from its base and then adds specific brain tumor watermark elements to HWS-CSIWT-activated images. Security measures for patient data transmission are established by applying this procedure, which helps protect information while ensuring medical data privacy in medical applications. The HWS system safeguards image confidentiality throughout the IoMT data transfer process, meeting healthcare needs for protected information transfer. The brain tumor extraction process obtains clarity through AGAN, which focuses on important diagnostic aspects. The application of HGGO-GA to segmented images fulfills the requirement of extracting the optimal features needed to differentiate between brain tumor pathological aspects. Medical data security combined with diagnostic precision improvement is the main objective, serving to create a complete system that provides safe data transfer while enhancing both patient care and clinical decisions.

The paper is structured into four key sections: Section 1 provides the introduction and related literature survey, Section 2 details the proposed methodology, Section 3 presents the experimental results and analysis, and Section 4 concludes the study and outlines future directions.

2. Proposed Secured Brain Tumor Classification Network

Medical-imaging technology has become vital in disease diagnosis and treatment following major advances in recent times, especially regarding neurological conditions. The advanced detection and classification of brain tumors has been achieved through modern technology-oriented methods. Medical data transmission through the IoMT depends on secure and efficient methods because healthcare operations now rely heavily on this communication technology. The proposed research presents a total framework that delivers proper diagnosis solutions. Table 1 outlines in sequence all the algorithm steps of the suggested framework. The proposed methodology's framework in Fig. 1 provides security measures for brain tumor image transfers through the IoMT while establishing a diagnostic tool that maintains reliable performance for medical practitioners. First, the research addresses the essential matter of safeguarding user privacy and maintaining confidentiality. A hypothetical patient case with a brain tumor diagnosis serves as the basis for testing the user message scenario of this system. The research selects a non-sensitive medical image for its cover role to protect patient confidentiality. Two distinct images are utilized in this project, with the brain tumor watermark image embedded inside the chosen cover image. The hidden watermark image contains the indicator of brain tumor presence in the transmitted information [41].

The implementation of HWS using CSIWT follows this procedure. HWS builds on the advantages of watermarking and steganography to provide safe and secure application of the watermark image inside the cover image. CSIWT improves watermarking security through its ability to represent image spatial data effectively. The constructed watermarked medical image displays brain tumor specifics in embedded form but appears exactly like an ordinary medical image, preserving confidentiality. The research now explores secure data transmission over the IoMT using the developed watermarked image. The system provides medical devices with a mechanism to exchange critical healthcare data between distributed platforms, enabling healthcare workers to obtain the required information remotely. The framework provides both integrity and confidentiality protection regarding transmitted brain tumor images while addressing security risks against medical data that exist in IoMT systems.

The watermarked image travels to its destination, where the embedded message-retrieval process occurs through an inversion step. The Inverse CSIWT-HWS system performs the inverse procedure of hybrid watermarking steganography by using CSIWT. Doctors receive vital information about brain tumor patients through this process, which reveals the incorporated watermark image. Medical professionals gain access to the original brain tumor image in addition to its extraction to analyze the tumor region. The OBTSC-Net provides advanced diagnostic performance capabilities. The model applies deep-learning approaches to segment different types of brain tumors from analyzed images precisely. The OBTSC-Net system employs state-of-the-art neural architecture structures, training strategies, and optimization approaches to perform precise brain tumor identification and classification.

The initial operation of the OBTSC-Net begins with applying AGAN to extract MRI brain tumor images. The generative model known as AGAN contains attention mechanisms that enable the network to focus on important regions of interest. The AGAN operation enhances extracted tumor image quality by displaying critical elements while lowering unimportant information. Precise image acquisition through this process becomes essential for subsequent research analysis.

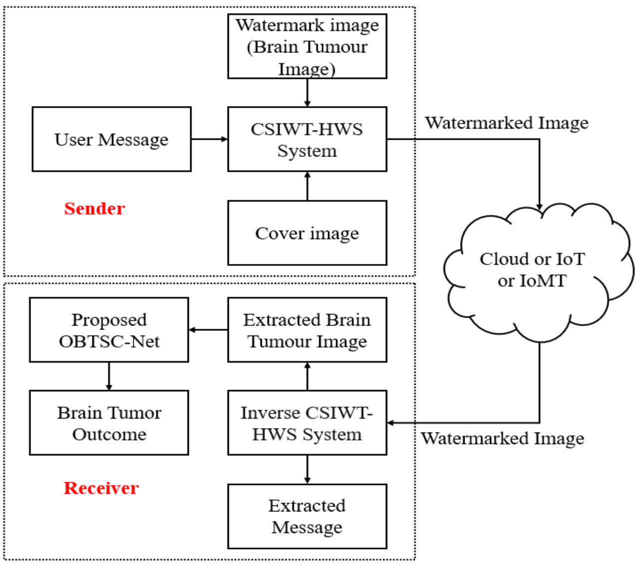

Fig.1. Proposed secured brain tumor classification network

The localization process of brain tumor images begins with subsequent HGGO-GA implementation on the separated image. Medical image analysis relies heavily on segmentation, as this process divides images into distinguishable portions utilizing meaningful fields. The segmented images pass through HGGO-GA, which enables the extraction of disease-specific optimal features. Genetic algorithms serve as optimization methods that use natural selection principles to identify relevant brain tumor features with hierarchical grouping optimization approaches. An essential step in obtaining discriminative features to characterize brain tumor pathology aspects must be performed.

The disease-specific optimal features extracted by HGGO-GA will later be used for benign and malignant brain tumor classification through BLS-NN. The neural network BLS-NN serves brain-lesion segmentation and classification tasks specifically. The BLS-NN receives features obtained from HGGO-GA and then uses a neural network structure to perform benign–malignant tumor distinction. During the training phase, the BLS-NN employs labeled datasets to discover patterns within extracted features, enabling it to generate accurate predictions throughout classification operations.

Table 1. Proposed secured brain tumor classification network algorithm

Input: Source MRI brain image, cover image, message **Output:** Watermarked image, Segmented image, Classified outcome. **Performance metrics:** Watermarking, segmentation, and classification.
Step 1: Consider the message (ex, the patient has a brain tumor), cover image, and watermark image (brain tumor image) from the user.
Step 2: Perform the HWS System using CSIWT, which hides the message and the user's brain tumor image in the cover image.
Step 3: The resultant watermarked image from CSIWT-HWS transmitted over the IoMT environment.
Step 4: Transmit the watermarked image in a secure environment using IoMT.
Step 5: Perform an Inverse CSIWT-HWS operation at the receiver's side on the watermarked image, which generates the original brain tumour image and message.
Step 6: Perform the OBTSC-Net operation to generate the disease classification outcome using a segmented image and optimal features. • Perform AGAN operation on extracted MRI brain tumor images, localizing the brain tumor area. • Apply HGGO-GA on segmented images to extract disease-specific optimal features. • Apply the BLS-NN on HGGO-GA extracted features, which classify benign and malignant brain tumors.
Step 7: Measure various performance metrics' watermarking, segmentation, and classification.

2.1. Hybrid Watermarking Steganography Embedding

CSIWT is a powerful technique that combines compressive sensing principles with integer wavelet transformation to represent and reconstruct signals [42, 43] efficiently. Compressive Sensing is a signal processing paradigm that enables the acquisition of sparse or compressible signals at a rate significantly lower than the Nyquist rate. The fundamental idea is that a signal is accurately reconstructed from fewer samples than traditionally believed. This ability benefits applications with limited data acquisition, storage, or transmission resources. This integration enables the efficient representation and reconstruction of signals, particularly those that exhibit sparsity. Consider a signal of length. A signal is deemed sparse if effectively represented in a sparse domain. Mathematically, this sparse representation is expressed as follows:

$$x = \Psi\alpha \tag{1}$$

Here, Ψ is a transformation matrix, and α is a sparse coefficient vector. The compressive sensing measurement model introduces the concept of acquiring compressed measurements (y) of the sparse signal (x) using a measurement matrix (Φ):

$$y = \Phi x \tag{2}$$

The integration of Compressive Sensing with Integer Wavelet Transform involves leveraging the sparsity-enabling properties of CS and the efficient multi-resolution analysis provided by IWT. The measurement matrix Φ in CSIWT is crucial in capturing the sparse representation of the signal in the wavelet domain. The choice of Φ significantly influences the success of the subsequent reconstruction algorithm. Once the compressed measurements (y) were obtained, the sparse signal (α) was recovered by solving an optimization problem that incorporates both the measurement matrix and the transformation matrix:

$$\alpha_{recovered} = \arg\min_{\alpha} |y - \Phi\Psi\alpha|_2^2 + \lambda\, |\alpha|_1 \tag{3}$$

In this equation, $|\alpha|_1$ represents the $\ell 1$-norm of α, and λ serves as a regularisation parameter, controlling the trade-off between fidelity to the measurements and sparsity of the signal. The final step involves reconstructing the original signal (x) from the recovered sparse coefficients ($\alpha_{recovered}$) using the inverse wavelet transform:

$$x_{recoverd} = \Psi^T \alpha_{recovered} \tag{4}$$

The compression process depends on the transformation matrix Ψ to transform sparse coefficients into the original signal. The core principle of this process includes creating an accurate representation of signals within sparse domains through compressive sensing principles. The measurement matrix Φ allows compressed measurement acquisition, which is then followed by an optimization process to retrieve sparse coefficients.

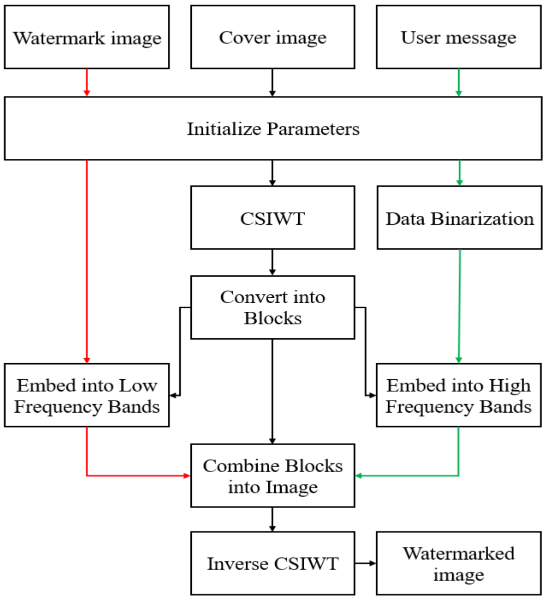

Fig.2. Proposed hybrid watermarking steganography embedding block diagram

Fig. 2, is a block diagram of the proposed HWS embedding algorithm. The algorithm for imprinting HWS is provided in Table 2. The following is the algorithm for watermarking medical images, specifically a brain tumor image and a message inserted by the user into the non-sensitive hosts. The purpose is to hide the information, so the normal eye cannot distinguish an alteration of the medical image. The actual image remains intact and secure.

In the first step, the algorithm invokes initialization and compression ratios that occur at the entrance of the CSIWT and determines the wavelet employed in the transformation and the strength employed in the watermarking process. These parameters are significant for understanding that the watermark is difficult to perceive or filter by possible attacks.

The second step entails applying the IWT to the cover image selected from the chosen wavelet. Subsequently, compression sensing is applied to the obtained wavelet coefficients following the targeted level of compression. This step assists in reducing the data content while ensuring that important information is retained in the watermarking process, making the process efficient.

Table 2. Proposed hybrid watermarking steganography embedding algorithm

Input: User message (e.g., patient details, diagnosis), Cover image (non-sensitive medical image), Watermark image (brain tumor image) **Output:** Watermarked image **Performance metrics:** Watermarking metrics.
Step 1: Initialize Parameters: • Set the compression ratio for CSIWT. • Choose a suitable wavelet for the transformation. • Define the embedding strength for watermarking.
Step 2: Transform the Cover Image Using CSIWT: • Apply the IWT to the cover image using the chosen wavelet. • Perform compressive sensing on the wavelet coefficients with the specified compression ratio.

Step 3: Embed the Brain Tumor Image:
• Divide the transformed cover image into blocks.
• For each block:
    • Extract a block from the brain tumor image.
    • Embed the block into the corresponding block of the transformed cover image in low-frequency bands.
    • Adjust the embedding strength to balance imperceptibility and robustness.

Step 4: Embed the User Message:
• Convert the user message into a binary representation.
• Divide the transformed cover image into suitable blocks.
• For each block:
    • Embed a portion of the binary message into the block in high-frequency bands.
    • Adjust the embedding strength to maintain invisibility.

Step 5: Inverse Transform: • Apply the Inverse CSIWT to obtain the watermarked image. • This step reconstructs the image with the embedded brain tumor blocks and the hidden user message.
Step 6: Output: The final watermarked image contains the hidden user message and the embedded brain tumor image within the cover image.

Second, the brain tumor image is incorporated into the stego area of the cover image. It splits the transformed cover image into regions and removes the corresponding region of the brain tumor image. The embedding process also operates in low-frequency bands, since the visibility of the watermark is minimized. The desirable level of embedding for the watermark is balanced, so the watermark should not be hidden and very difficult to remove.

After transforming the cover image, the algorithm embeds the user message in the blank reconstructed image of the brain tumor. The user message is encoded in binary form, and the transformed cover image is divided into effective blocks. The binary message is implanted in the high-frequency bands of each block, and only for the third time is the embedding intensity changed to make it secretive.

The fifth process involves applying the reverse CSIWT to view the watermarked image. This step is important in reconstructing the image, which contains the blocks of the brain tumor and the hidden message of the user. The inverse transform helps make the watermarking process reversible when the option arises to extract the watermarked information into the original form.

2.2. IoMT

In the proposed HWS system, the IoMT plays a pivotal role in the secure transmission and accessibility of watermarked medical images. After the Inverse CSIWT-HWS operation generates the original brain tumor image and user message, the IoMT facilitates the seamless communication of these critical medical data between the healthcare provider and the relevant medical professionals. Leveraging the IoMT, the reconstructed brain tumor image and the user message are securely transmitted over networked devices, enabling remote diagnostics, collaboration, and timely decision-making. This integration enhances the efficiency of healthcare services by allowing medical practitioners to access and analyze essential patient information in real time, regardless of geographical constraints. The IoMT, serving as the support system for interconnected medical devices and systems, contributes to the advancement of telemedicine and ensures that the benefits of the HWS system are extended beyond the confines of a single medical facility.

2.3. Hybrid Watermarking Steganography Extraction

The proposed HWS extraction algorithm detailed in Table 3 provides a systematic approach to recovering the original brain tumor image and user message from a watermarked image [44,45]. Fig. 3 provides a graphical representation of the HWS extraction process. In addition, the main purpose is to demoralize, with minimal losses for the embedded information, depending on the type of watermarking used in the working area.

First, the algorithm takes the initial conditions and uses them to set the compression ratio of inverse CSIWT and the type of wavelet used for the HWS process. These parameters help retrieve the original information hidden in the watermarked image. The second process involves applying the CSIWT to a watermarked image. This process is a reverse operation performed on a watermark, which provides an image with the embedded blocks of the brain tumor and the concealed user message.

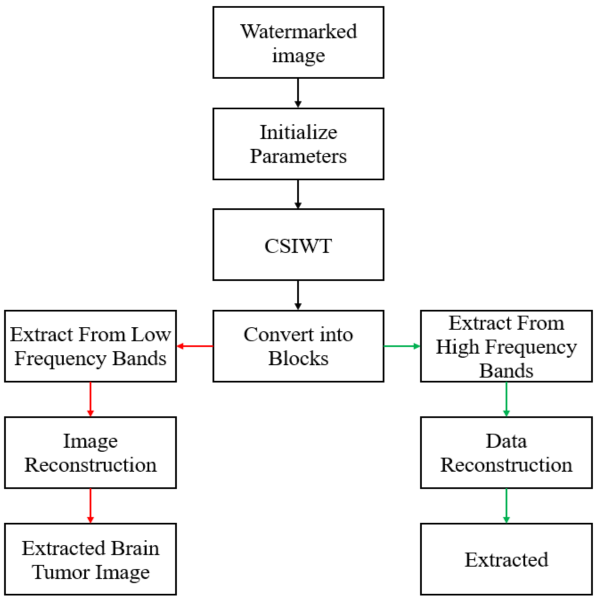

Fig.3. Proposed hybrid watermarking steganography extraction block diagram

Third, the algorithm uses back transformation to retrieve the brain tumor blocks from the transformed image by segmenting the image following transformation and identifying each block's intrinsic brain tumor data in the low-frequency bands. All the extracted blocks help reconstruct the complete image of the brain tumor.

Fourth, the hidden user message is retrieved from the transformed image by splitting that image into blocks and extracting the data of the user's message from the high-frequency bands. The separate message portions of the extracted messages are then joined to reconstruct the original user message. Therefore, the final determined results involve reconstructing the original brain tumor image and the retrieved user message. The performance of the extraction process is assessed based on the following watermarking metrics, as pointed out by performance metrics. This comprehensive extraction algorithm ensures the recovery of the medical image and user message, demonstrating its efficacy in reversing the watermarking and steganography operations applied to the input watermarked image.

Table 3. Proposed hybrid watermarking steganography extraction algorithm

Input: Watermarked image. **Output:** Original brain tumor image, User message. **Performance metrics:** Watermarking metrics.
Step 1: Initialize Parameters: • Set the compression ratio for the inverse CSIWT. • Choose the wavelet used in the HWS operation.
Step 2: Apply CSIWT Transform: Apply the CSIWT to the watermarked image to obtain the transformed image with the embedded brain tumor blocks and hidden user message.
Step 3: Extract Brain Tumor Blocks: • Divide the transformed image into blocks. • For each block: Extract the embedded brain tumor data from low-frequency bands.
Step 4: Reconstruct Brain Tumor Image: Combine the extracted brain tumor blocks to reconstruct the original brain tumor image.
Step 5: Extract User Message: • Divide the transformed image into blocks. • For each block: Extract the hidden user message data from high-frequency bands.
Step 6: Reconstruct User Message: Combine the extracted message portions to reconstruct the original user message.
Step 7: Output: The final outputs are the original brain tumor image and the extracted user message.

2.4. Brain Tumor Segmentation

The AGAN approach is a sophisticated model designed for brain tumor image segmentation. Fig. 4 illustrates the proposed AGAN architecture, and Table 4 contains the algorithm steps. At the core of AGAN lies the attention mechanism, a critical component that enables the model to focus on relevant regions while generating or segmenting images. The attention mechanism mathematically assesses the importance of different spatial locations in the input image [46,47]. Let represent the input brain tumor image and denote the corresponding ground truth segmentation mask. The attention mechanism is characterized by equations determining the attention weights assigned to different spatial locations in the input image. Let represent the attention weights matrix and denote the feature map. The attended feature map F_a is computed as follows:

$$F_a = A \odot F \tag{4}$$

Here, $\odot$ denotes element-wise multiplication. The attention weights are measured based on the correlation between the input image and the features that influence the model's ability to focus on the areas related to brain tumors. In the generator part of AGAN, the segmentation image is obtained by combining the input image and the feature map that has been attended. The mathematical model of the generator involves convolutions and sampling operations that concern the inputs and produce a segmentation map using the attention mechanism, which emphasizes features related to the brain tumor areas. The generator is represented as follows:

$$G(X) = Segmentation\,Map \tag{5}$$

Generate the segmented image $\hat{Y}$ using the original input X and the attended feature map F_a.

$$\hat{Y} = G(X, F_a) \tag{6}$$

The discriminator evaluates the realism of the generated segmented images by comparing them with the ground truth masks. The adversarial loss (L_{adv}) is computed as the discrepancy between the generated and real segmented images:

$$L_{adv} = -E_Y[\log D(Y)] - E_{\hat{Y}}\left[\log\left(1 - D(\hat{Y})\right)\right] \tag{7}$$

Here, D represents the discriminator, and the expectations (E_Y, $E_{\hat{Y}}$) take over the authentic and generated segmented image distribution. The discriminator aims to maximize L_{adv} to distinguish between authentic and generated images, whereas the generator aims to minimize it. Compute the generator's adversarial loss to guide the generator in producing realistic segmented images.

$$L_{gen} = -E_{\hat{Y}}\left[log\ D\left(\hat{Y}\right)\right] \tag{8}$$

AGAN refines its parameters throughout the training process by optimizing the attention mechanism. The generator learns to produce segmented images that closely match the ground truth masks, and the discriminator becomes more adept at distinguishing between authentic and generated images. The attention mechanism dynamically guides the generator to focus on critical regions, effectively segmenting brain tumors. Finally, the trained generator network (G) can generate segmented brain tumor images.

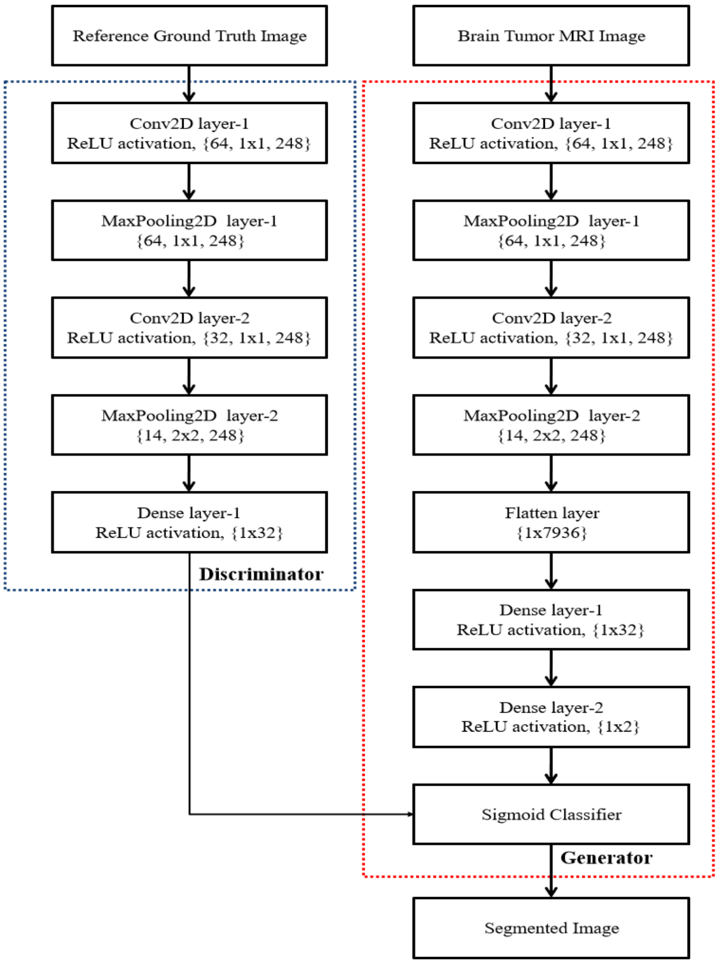

Fig.4. Proposed attention generative adversarial network segmentation algorithm

Table 4. Proposed attention generative adversarial network segmentation algorithm

Input: Input brain tumor image (X), Reference segmentation mask (Y). **Output:** Segmented tumor Image. **Performance Metrics:** Segmentation metrics.
Step 1: Initialize the parameters of the generator network *G* and discriminator network *D*.
Step 2: Attention Mechanism: Compute the attention weights matrix *A* using the input image *X* and its features *F*.
Step 3: Generator Network: Generate the segmented image $\hat{Y}$ using the original input image X and the attended feature map F_a.
Step 4: Discriminator Network: Using discriminator network D, evaluate the realism of both objective (Y) and generated $(\hat{Y})$ segmented images.
Step 5: Update Discriminator Parameters: Minimize the adversarial loss (L_{adv}) by updating the parameters of the discriminator network.
Step 6: Generator Adversarial Loss Compute the generator's adversarial loss to guide the generator in producing realistic segmented images.
Step 7: Update Generator Parameters: Update the Generator network parameters to minimize the adversarial loss (L_{gen}).
Step 8: Repeat Training Iterations: Repeat Steps 2 to 7 for a predefined number of training iterations until the generator produces realistic and accurate segmented images.

2.5. Optimal Feature Extraction

The optimal feature-analysis process encompasses the input parameters, initialization, objective function, encoding of features, optimization process, genetic algorithm integration, local search mechanism, and the final output. The mathematical equations capture the essence of each phase within the HGGO-GA approach for optimal feature extraction from segmented brain tumor images [48]. This integrated algorithm aims to balance exploration and exploitation, leveraging the strengths of both optimization techniques to identify feature subsets that enhance classification performance in brain tumor images.

Fig. 5 is the HGGO-GA flowchart. Table 5 contains the HGGO-GA algorithm process for optimal feature extraction. The algorithm begins by considering the input parameters, including the segmented brain tumor images dataset D, label information L, population size N, the maximum number of generations G, inertia weight w, acceleration coefficients c_1 and c_2, and probabilities of crossover p_c and mutation p_m. The initialization phase then establishes the initial positions of N geese in the feature space. The position of each goose i is encoded as a binary vector $Position_{i,j}$, where j denotes the feature index. This binary encoding signifies the presence or absence of specific features in the subset.

Objective Function and Encoding Features: The core of the algorithm lies in the definition of the objective function, representing the fitness of each goose's position. This fitness function is designed to evaluate the quality of a given subset of features. Mathematically, the objective function takes the following form:

$$J(Position_i) = FF(D, L, Position_i) \tag{9}$$

Here, the fitness metric evaluates the classification performance based on the chosen subset of features. Additionally, the encoding of features is represented by binary vectors, in which each element $Position_{i,j}$ is either 1 (indicating the selection of the j^{th} feature) or 0 (indicating its absence).

Optimization Process: The optimization loop spans G generations, in which the fitness of each goose is evaluated based on the objective function. The global best goose is updated, and genetic operations are applied, including selection, crossover, and mutation. In the selection phase, geese are chosen for crossover based on their fitness. A common approach is tournament selection, in which individuals compete in randomly selected groups, and the winner is chosen for crossover. The crossover operation involves exchanging features between pairs of geese. The probability of crossover () determines whether the features are exchanged, and if not, the features are inherited from the global best goose (). The mathematical representation of crossover is expressed as follows:

$$Position_{i,j}^{off} = \begin{cases} Position_{i,j}, & with\,probability\; p_c \\ Position_{g_{Best},j}, & with\,probability\; 1 - p_c \end{cases} \tag{10}$$

In the mutation phase, each goose undergoes mutations with a certain probability (p_m). Mutation introduces diversity by flipping or changing features in the position vector. The mutation operation is mathematically defined as follows:

$$Position_{i,j}^{mut} = \begin{cases} 1 - Position_{i,j}, & with\,probability\; p_m \\ Position_{g_{Best},j}, & with\,probability\; 1 - p_m \end{cases} \tag{11}$$

The threshold function then converts the resulting positions into binary values, maintaining the binary encoding.

Update Velocity and Position: Following the genetic operations, the velocity and position of each goose are updated using the GGO algorithm's velocity equation. The velocity equation incorporates the inertia weight (w), acceleration coefficients (c_1, c_2), and random values (rand1, rand2).

Mathematically, the velocity update equation is expressed as follows:

$$Velocity_{i,j} = w \times Velocity_{i-1,j-1} + c_1 \times rand1 \times \left(p_{Best_{i,j}} - Position_{i,j}\right) + c_2 \times rand2 \times \left(g_{Best_j} - Position_{i,j}\right) \tag{12}$$

Here, $p_{Best_{i,j}}$ represents the best position of the current goose i in the j-th dimension, and g_{Best_j} denotes the best position among all geese in the j-th dimension. The change in velocity also affects the velocity of the goose in the feature space. Then, the position of each goose is changed according to the computed velocity accordingly:

$$Position_{i,j} = Position_{i-1,j-1} + Velocity_{i,j} \tag{13}$$

An example of a change in position is then used to illustrate how the threshold function is subsequently used to convert all positions to binary so that their form is preserved as the optimization is made.

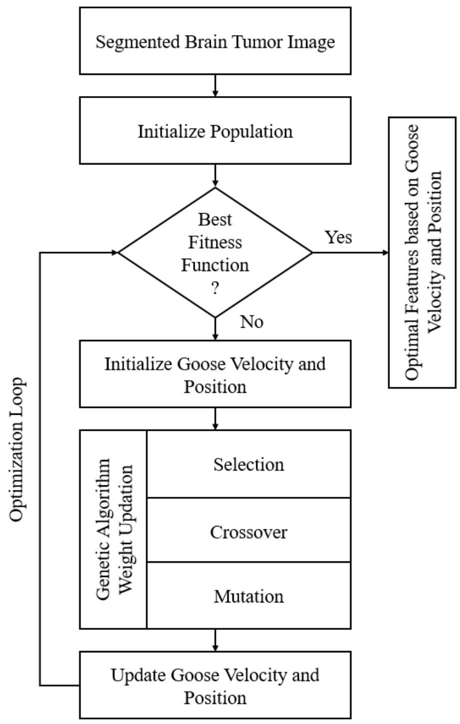

Fig.5. Proposed hybrid grey-lag goose optimization-based genetic algorithm

Table 5. Proposed hybrid greylag goose optimization-based genetic algorithm

Input: Segmented brain tumor image, GGO Parameters. **Output:** Optimal features.
Step 1: Initialize Population: Randomly initialize N geese with binary positions in the feature space.
Step 2: Define the fitness function $of\ J(Position_i)$, which evaluates the quality of each goose's position.
Step 3: Initialize the optimization loop and repeat for t=1 to G.
Step 4: Evaluate the fitness of each goose based on its position: $J(Position_i)$.
Step 5: Update the global best goose based on the goose with the highest fitness.
Step 6: Apply genetic operators (selection, crossover, and mutation) to update the geese's positions and weights. **Selection:** Choose geese for crossover based on fitness (e.g., tournament selection). **Crossover**: For each selected pair of geese, perform crossover with probability p_c. **Mutation:** For each goose, perform mutation with probability p_m. Apply a threshold function to convert positions into binary values.
Step 7: Update Velocity and Position: Update the velocity using the GGO velocity equation. Update the position using the updated positions from the genetic operators. Apply a threshold function to convert positions into binary values.
Step 8: Terminate the optimization loop after reaching the best fitness function.
Step 9: The binary vector of the global best goose represents the optimal subset of features for brain tumor image classification.

Finally, it is the integration of genetic operations into the GGO algorithm which improves the features of exploration and exploitation. The evaluation of selection, crossover, and mutation in gene pulls and selection also helps the algorithm to search the solution space efficiently. The p_c and p_m are the parameters controlling the level of exploration and exploitation in the algorithm. Thus, based on the merged GGO and genetic algorithms, the algorithm can find a better feature subset to classify brain tumor images. In addition to the basic genetic function, there must exist a local search regarding a specific vicinity around the current solution. The local search is a refinement of the position of a goose within a given level of the local search domain. It was done based on the specific exploration strategy in use, and the mathematical formulation of the local search also depends on the exploration strategy in place. The result of the algorithm is the binary vector of the globally best goose, which holds the optimal features to classify brain tumor images. Such binary vectors demonstrate the selected features that provide the maximum classification capability.

2.6. Broad Learning System Classifier

The BLS-NN is designed to address the challenges posed by big data analytics, particularly in high-dimensional feature spaces, such as those encountered in brain tumor classification [49]. Fig. 6 illustrates the BLS-NN architecture, and Table 6 contains the algorithm procedure of the proposed BLS-NN classifier. Initially, let represent the original feature matrix derived from the HGGO-GA module. A set of M features is extracted and denoted as $X_{selected} \in R^{N\times M}$.

The output of a BLS-NN for a given set of features $X_{selected}$ is expressed as follows:

$$Y_i = \phi(X_{selected} \cdot W_i + B_i) \tag{14}$$

Here, Y_i represents the output of the i-th BLS-NN layers, ϕ is the activation function, W_i denotes the weight matrix, and B_i is the bias vector. The activation function introduces non-linearity to the BLS-NN's output, enabling the network to model complex relationships in the data. The training goal is to minimize the loss function L over the training dataset, in which Y represents the predicted output of the BLS model, and $\hat{Y}$ represents the ground truth labels. Minimizing the loss function helps the model learn to make accurate predictions. Backpropagation is used to update the weights of the BLS-NNs based on the gradient of the loss function concerning the weights. The learning rate η determines the weight update size, influencing the training process's convergence and stability.

$$W_i^{new} = W_i^{old} - \frac{\eta \partial L}{\partial W_i} \tag{15}$$

Furthermore, L2 regularization is applied to the loss function to prevent overfitting by penalizing large weights. The regularization parameter λ controls the strength of regularization, influencing the trade-off between fitting the training data and generalizing to unseen data.

$$L_{regularized} = L + \lambda \sum_{i=1}^{N} |W_i|_2^2 \tag{16}$$

The fusion weights α_i are updated using gradient descent to minimize the loss function. These weights control the contribution of each BLS-NN to the ensemble output, enabling the model to assign importance to different BLS-NNs adaptively during the classification process.

$$\alpha_i^{new} = \alpha_i^{old} - \frac{\eta \partial L_{regularized}}{\partial \alpha_i} \tag{17}$$

The ensemble output Y is computed as a weighted combination of the outputs of all BLS-NN layers and the SoftMax classifier. This equation allows the BLS model to leverage the collective knowledge of multiple BLS-NN layers for improved classification performance.

$$Y = \sum_{i=1}^{N} \alpha_i^{new} Y_i \tag{18}$$

Finally, output Y contains the brain tumor's classified outcomes as benign and malignant.

Table 6. Proposed broad learning system neural network algorithm

Input: Optimal features from HGGO-GA. **Output:** Brain tumor classified outcome.
Step 1: Initialize the feature matrix X derived from the HGGO-GA module.
Step 2: BLS-NN output calculation for each layer i, calculate the output Y_i.
Step 3: Define the loss function L over the training dataset.
Step 4: Use backpropagation to update the weights of the BLS-NNs based on the gradient of the loss function concerning the weights.
Step 5: Apply L2 regularization to the loss function to prevent overfitting.
Step 6: Update the fusion weights α_i using gradient descent to minimize the regularized loss function.
Step 7: Calculate the ensemble output Y as a weighted combination of SoftMax classifier and other BLS-NNs.
Step 8: The final output Y contains the brain tumor classified outcome, such as benign and malignant.

3. Results and Discussion

This section presents an in-depth examination of the simulation outcomes conducted within the MatlabR2021a software environment. The proposed methodology's efficacy is scrutinized using established models, employing a range of performance metrics. The evaluation assesses and compares HWS, segmentation, and classification performances. To manage this complexity and ensure feasible training times, all implementations both proposed and comparative methods were executed on a high-performance Intel i9 CPU system with GPU acceleration and 32 GB RAM. This setup reflects a realistic academic environment for medical AI research and supports high-speed model training and evaluation. Despite the layered architecture, the system remains computationally practical for modern healthcare research labs.

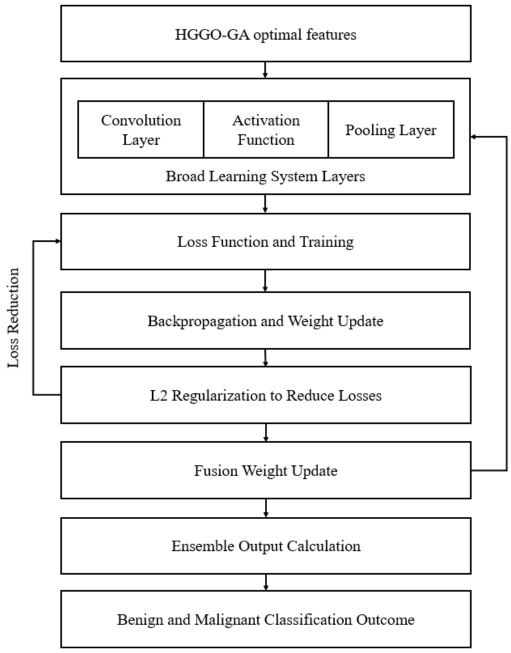

Fig.6. Proposed broad learning system neural network flow diagram

3.1. Dataset

This section presents the outcomes of applying our proposed model to two widely recognized datasets, BraTS-2020 and BraTS-2021, integral parts of the MICCAI challenge [50]. Precisely, the RSNA-ASNR-MICCAI BraTS 2021 dataset consists of 2040 data samples. Within this dataset, 1251 samples are allocated for training, and 219 samples are designated for validation through synapse.org. Each data sample is characterized by four 3D MRI sequences, namely T1, T1-gd, T2, and T2-FLAIR, all about a single subject. The dimensions of each 3D-MRI modality are consistent at $240 \times 240 \times 155$, and the multiparametric mp-MRIs are acquired using diverse scanners and methods across various institutions. Notably, the isotropic voxels maintain $1 \times 1 \times 1$ mm^3 dimensions.

The dataset undergoes expert annotation, delineation, and segmentation by radiologists to establish the training set's ground truth (mask). This process results in e-subregions of tumors, specifically labeled as "tumor core TC" for necrotic and non-enhancing tumors, "whole tumor WT" for peritumoral edema, and "ET" for enhancing tumors. Each tumor subregion describes the distinct behavior and characteristics of the tumor. For instance, the T1-Gd modality exhibits a hyper-intense signal in the ET subregion, whereas the NET and NCR subregions appear hypo-intense compared to the T1 modality. The combination of NET and NCR, peritumoral edema (ED), and the tumor core (TC) forms the whole tumor (WT), comprehensively representing the tumor's overall extent and size.

The dataset specifications for BraTS 2020 and BraTS 2021 are summarized as follows. Regarding BraTS 2020, the input image size is standardized at $240 \times 240 \times 155$ voxels. This dataset comprises 369 data samples allocated for training and 125 samples designated for validation. On the other hand, regarding BraTS 2021, the input image size remains consistent at $240 \times 240 \times 155$ voxels. However, this dataset is notably larger, containing 1251 data samples for training and 219 samples for validation.

3.2. Subjective Evaluation

Fig. 7 illustrates the outcomes of the proposed HWS-CSIWT, highlighting the critical stages of the algorithm and its implications for security and privacy in the context of the user message ("Patient Had Brain Tumor Symptoms"). The process begins with a source brain tumor image, denoted as Fig. 7(a), representing the original medical data containing information about the patient's brain tumor symptoms. A cover image is selected, represented in Fig. 7(b), to ensure the confidentiality and secure transmission of this sensitive information, which serves as the basis for embedding both the user message and the brain tumor image watermark. The HWS-CSIWT process is then applied to these images, creating watermarked images, as Fig. 7(c) indicates. This step involves transforming the cover image using CSIWT, embedding the brain tumor image within the transformed cover image, and hiding the user message through steganography techniques. The watermarked images encapsulate both the visual representation of the brain tumor and the textual information about the patient's condition, ensuring a seamless integration of diagnostic data. The extraction phase, denoted as Fig. 7(d), illustrates the reverse process at the receiver end. The watermarked images are subjected to an Inverse CSIWT-HWS operation, extracting the original brain tumor image and the user message. The extracted source images, depicted in Fig. 7(d), represent the successful retrieval of the underlying medical data, maintaining the integrity of the visual and textual information related to the patient's brain tumor symptoms. The user message "Patient Had Brain Tumor Symptoms" is prominently highlighted, emphasizing the critical diagnostic information's successful transmission and retrieval.

Fig. 8 illustrates a comparison between the embedding performance of the current methods and the HWS-CSIWT. Fig. 8(a) is of ECDSA [41], which is an outcome of the digital signature algorithms that have robust security measures. However, the signs indicate problems concerning color balance, which is an issue that highlights that the attacks negatively affect the outer look of the embedded information. Furthermore, Fig. 8(b) presents the Convolutional Attention-based Turtle Shell Matrix (CATSM), which is one outcome of this specifically customized embedding technique that uses convolutional attention mechanisms. In addition, the aspects of color balance are questionable, suggesting that attacks affect the quality and credibility of the incorporated information.

Fig. 8(c) presents the result of the Vigenere Cipher Algorithm with Least Significant Bits (VCA-LSB) [43], reflecting the integration of classical cryptography and steganography. The existence of this method leaves room for color balance attacks, which is a potential threat to and compromise of the visual representation of the entire embedded information. Regarding the qualitative comparison of the HWS-CSIWT, the proposed algorithm excelled specifically in the aspect of embedding performance. The graph reveals that this approach minimizes problematic color balance; thus, it is more resistant to attacks. The framework of HWS-CSIWT incorporated in Fig. 8(d) is highly resilient due to the use of CS and IWT, in addition to the capability of providing a secure and visually vivid method of hiding information inside medical images.

Fig. 9 is a comparison of different approaches of extraction performance from methods other than HWS-CSIWT. Binarization problems occurred during the extraction, as depicted in Fig. 9(a), regarding the extraction performance of ECDSA [40]. Various problems are associated with binarization, since it is impossible to extract the concealed message perfectly, as it is sometimes distorted or eradicated. Fig. 9 (b) illustrates CATSM [41], which has greyscale issues during extraction. These issues result in discrepancies in the recovered image, affecting the embedded data's visual quality and grayscale fidelity. Fig. 9 (c) is of VCA-LSB [42] and reveals color-aliasing effects during extraction, suggesting challenges in accurately reconstructing the original color information. The proposed HWS-CSIWT is represented in Fig. 9(d), demonstrating favorable extraction performance. The absence of specific extraction issues indicates the robustness of the proposed method in accurately recovering the embedded information without introducing binarization, grayscale, or color-aliasing artifacts.

Fig. 10 illustrates various approaches to brain tumor segmentation performance, including existing methods and the proposed AGAN. Fig. 10(b) concerns SKM [23] segmented outcome, which is a method that combines saliency detection with K-means clustering for brain tumor segmentation. The segmentation outcomes of this approach are associated with incorrect results, suggesting potential challenges in accurately delineating tumor regions using the SKM method. Fig. 10(c) illustrates CNN [24] segmentation outcome, a deep-learning-based approach commonly employed for image segmentation tasks. It highlights potential issues with the segmentation outcomes of CNN, indicating that the results deviate from the ground truth and exhibit inaccuracies. Fig. 10(d) illustrates the LuNetClassifier [47] segmentation outcome, another classification-based method for brain tumor segmentation, and it suggests that the segmentation results produced by LuNetClassifier have incorrect outcomes, emphasizing potential limitations in accurately classifying tumor and non-tumor regions. The proposed AGAN, labeled in Fig. 10(e), is introduced as a novel approach for brain tumor segmentation. The outcomes of AGAN appear promising, suggesting improved segmentation performance compared with existing methods. Attention mechanisms and adversarial training contribute to a more accurate delineation of tumor regions.

3.3. Objective Evaluation

Table 7 presents a comprehensive performance comparison of various HWS methods, evaluating their effectiveness based on three key metrics: PSNR, Structural Similarity Index (SSIM), and Mean Squared Error (MSE). The methods under consideration are ECDSA [40], CATSM [41], VCA-LSB [42], self-recovery watermarking scheme (SRWS) [43], optimized wavelet transform (OWT) [44], and the proposed HWS-CSIWT.

Beginning with PSNR, the proposed HWS-CSIWT method exhibits a notable improvement over ECDSA [40], with a percentage improvement of 25.01%. Compared with CATSM [41], HWS-CSIWT demonstrated an improvement of 16.34%, and the improvement over VCA-LSB [42] was 9.81%. The improvement percentages relative to SRWS [43] and OWT [44] were substantial, with values of around 5.08% and 3.04%, respectively. The superior PSNR values of the proposed HWS-CSIWT method signify its ability to maintain high signal fidelity and minimize distortion during the embedding process. Regarding SSIM, the proposed HWS-CSIWT method revealed remarkable improvements across all the compared methods. Compared with ECDSA [40], the improvement was 16.94%. The percentage improvement over CATSM [41] was 12.85%, while the improvement over VCA-LSB [42] was notably higher at 11.18%. Compared with SRWS [43] and OWT [44], the proposed method demonstrated improvements of 4.90% and 4.74%, respectively. The higher SSIM values affirm the ability of HWS-CSIWT to preserve structural information and enhance the perceptual quality of watermarked images.

Regarding MSE, the proposed HWS-CSIWT method achieved significant improvements overall compared with other methods. Compared with ECDSA [40], the percentage improvement was 61.67%. The improvement over CATSM [41] was 58.85%, and 58.68% over VCA-LSB [42]. The percentage improvements over SRWS [43] and OWT [44] were substantial, with values of 56.16% and 37.73%, respectively. The lower MSE values attained by HWS-CSIWT indicate a more accurate reconstruction of the original images and a reduction in the mean squared differences between the original and watermarked images.

User Message: Patient Had Brain Tumor Symptoms

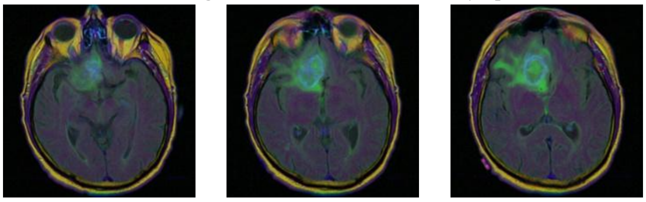

(a) source brain tumor images

(b) cover images

(c) watermarked images

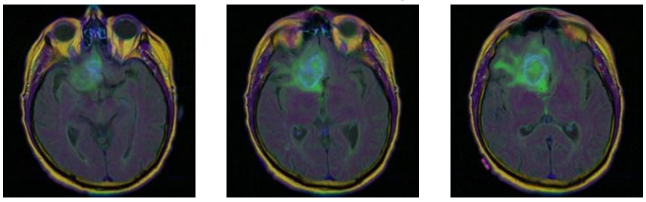

(d) extracted source images

Extracted Message: Patient Had Brain Tumor Symptoms.

Fig.7. Proposed HWS-CSIWT process outcomes

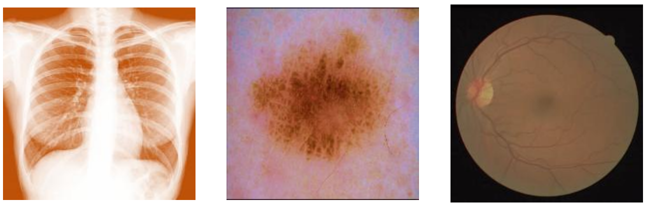

(a) ECDSA [40]

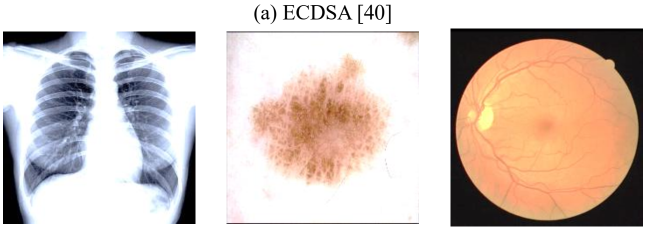

(b) CATSM [41]

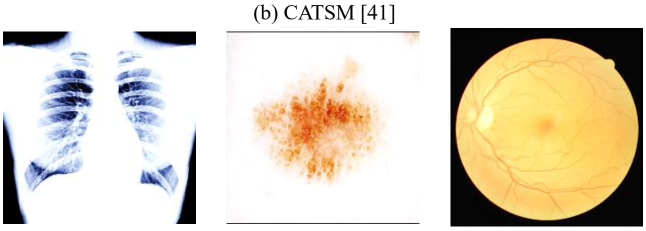

(c) VCA-LSB [42]

(d) proposed HWS-CSIWT

Fig.8. HWS-CSIWT embedding performance of various approaches

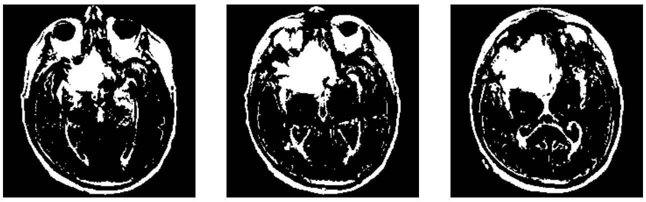

(a) ECDSA [40]

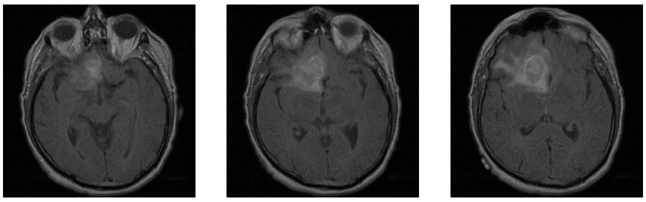

(b) CATSM [41]

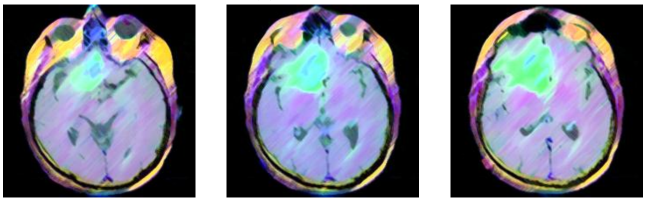

(c) VCA-LSB [42]

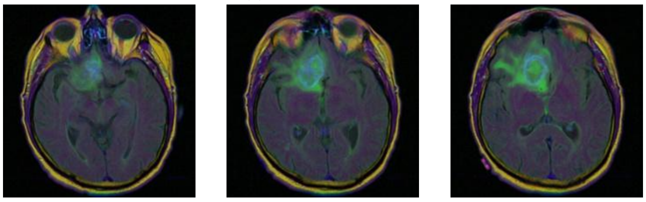

(d) proposed HWS-CSIWT

Fig.9. HWS-CSIWT Extraction performance of various approaches

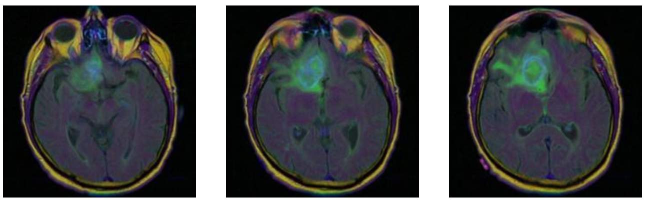

(a) source brain MRI images

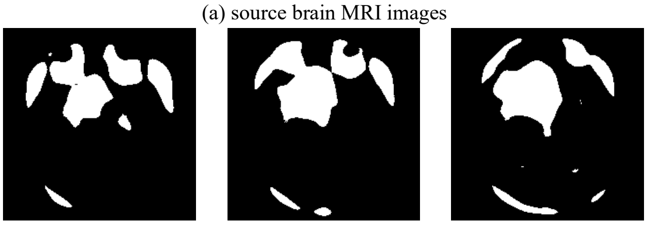

(b) SKM [23]

(c) CNN [24]

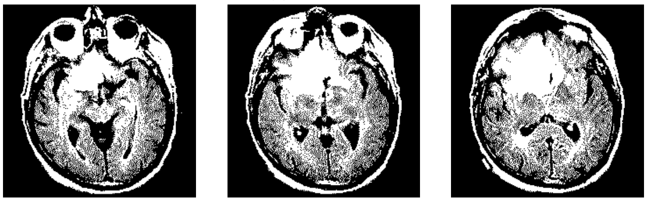

(d) LuNetClassifier [47]

(e) Proposed AGAN

Fig.10. Brain tumor segmentation performance of various approaches

Table 8 lists the assessment of the security performance of various HWS methods through four key metrics: Entropy, NPCR (Normalized Pixel Change Rate), NCC (Normalized Cross-Correlation), and UACI (Unified Average Change Intensity). The proposed HWS-CSIWT methodology was compared with existing methods: ECDSA [40], CATSM [41], VCA-LSB [42], SRWS [43], and OWT [44]. Regarding Entropy, the proposed HWS-CSIWT demonstrated a notable improvement of 45.54% compared with ECDSA [40], 29.32% compared with CATSM [41], 23.32% compared with VCA-LSB [42], 10.52% compared with SRWS [43], and 8.49% compared with OWT [44]. The results signify HWS-CSIWT's enhanced ability to increase unpredictability and information content in watermarked images.

Regarding NPCR, the proposed HWS-CSIWT method exhibited substantial improvements, surpassing ECDSA [40] by 27.79%, CATSM [41] by 23.47%, VCA-LSB [42] by 18.44%, SRWS [43] by 10.39%, and OWT [44] by 5.62%. A higher value of NPCR means a greater change in the pixel values and, thus, better security and immunity against attacks. Regarding NCC, HWS-CSIWT achieved an improvement of 15.07% over ECDSA [40], 11.98% over CATSM [41], 8.32% over VCA-LSB [42], 5.83% over SRWS [43], and 3.91% over OWT [44]. Based on these results, HWS-CSIWT provided a higher base linear relationship than the original and watermarked image, improving the correlation and fidelity. Furthermore, regarding UACI, the proposed HWS-CSIWT displayed substantial improvements, outperforming ECDSA [40] by 9.05%, CATSM [41] by 6.939%, VCA-LSB [42] by 5.507%, SRWS [43] by 4.056%, and OWT [44] by 3.042%. Higher UACI percentages emphasize HWS-CSIWT's superior ability to preserve image quality and ensure secure data embedding.

Table 7. Performance comparison of various HWS methods

Method	PSNR (dB)	SSIM	MSE
ECDSA [40]	60.384	0.8539	0.002174
CATSM [41]	63.384	0.8821	0.002038
VCA-LSB [42]	68.485	0.89393	0.001916
SRWS [43]	71.93	0.90183	0.001846
OWT [44]	72.48	0.95134	0.001333
Proposed HWS-CSIWT	75.47	0.9944	0.000833

Table 9 lists the evaluation of the segmentation performance comparison of all the methods involved regarding the parameters used. The compared methods are SKM [23], CNN [24], LUNET [47], DSM [46], and the proposed AGAN. Based on the SMCC metric, the proposed AGAN improved much more than all the other methods in this paper. Concerning the comparisons, AGAN was 2.94% better than SKM [23], 5.99% better than CNN [24], 2.984% better than LUNET [47], and, notably, 1.756% better than DSM [46]. The results demonstrate that AGAN has the potential to achieve a true-positive and true-negative ratio of brain tumor segmentation.

Regarding the Segmentation F1 Score (SF1) metric, which evaluates the performance of the arrays generated through payers and counts information, the proposed AGAN improved and stabilized by approximately 2.61% compared with SKM [23], 3.845% compared with CNN [24], 2.845% compared with LUNET [47], and, significantly, 1.664% compared with DSM [46]. Thus, AGAN achieved its targets in precision and recall more than other related methods regarding high F1 scores. AGAN was lower than SKM by 0.36%, lower than CNN by 5.973%, lower than LUNET by 1.122%, and lower than DSM by 1.919% regarding SFNR. It is due to the approach that AGAN reduced its false negatives to a minimum to achieve a high actual positive rate.

Table 8. Security performance of various HWS methods

Method	Entropy	NPCR (%)	NCC	UACI (%)
ECDSA [40]	40.84	27.845	0.8638	90.73
CATSM [41]	45.924	28.824	0.8916	92.845
VCA-LSB [42]	48.014	30.134	0.9132	94.277
SRWS [43]	53.959	32.194	0.9362	95.734
OWT [44]	54.58	33.956	0.9654	96.742
Proposed HWS-CSIWT	59.48	35.58	0.9945	99.784

The proposed AGAN also revealed enhanced SFDR by 0.22% compared with SKM [23], 0.374% compared with CNN [24], 1.378 % compared with LUNET [47], and 2.917% compared with DSM [46]. Furthermore, AGAN resulted in a reduced rate of false discoveries, improving the precision parameter of positive cases during segmentation. In general, regarding SFPR, the proposed AGAN achieved considerable enhancement: 5.852% more than SKM [23], 6.372% more than CNN [24], 4.172% more than LUNET [47], and 2.648% more than DSM [46]. The model's balanced precision and recall resulted in fewer false positives during brain tumor segmentation. The proposed AGAN excelled regarding SNPV (Segmentation Negative Predictive Value), with a 6.689% improvement over SKM [23], 4.121% over CNN [24], 2.107% over LUNET [47], and 2.254% over DSM [46]. The model's heightened accuracy in predicting negative cases contributes to its efficacy in segmentation.

Regarding SPR (Segmentation Precision Rate), the proposed AGAN achieved comprehensive improvements: 6.469% over SKM [23], 4.645% over CNN [24], 3.535% over LUNET [47], and 1.141% over DSM [46]. The enhanced precision of AGAN in identifying actual positive cases is evident. The model excelled regarding SPEC (Segmentation Specificity), with improvements of 6.196% over SKM [23], 5.674% over CNN [24], 3.967% over LUNET [47], and 0.859% over DSM [46]. The proposed AGAN's ability to identify negative cases contributes to its specificity in segmentation. The model demonstrated heightened sensitivity regarding SSEN (Segmentation Sensitivity), with improvements of approximately 7.976% over SKM [23], 4.307% over CNN [24], 3.324% over LUNET [47], and 1.355% over DSM [46]. AGAN's accurate identification of positive cases is a key strength. The model achieved overall SACC improvements, with 7.077% over SKM [23], 5.575% over CNN [24], 4.059% over LUNET [47], and 2.185% over DSM [46]. AGAN's effectiveness in achieving balanced and accurate brain tumor segmentation outcomes is evident across all metrics.

Table 9. Segmentation performance comparison of various methods

METRIC	SKM [23]	CNN [24]	LUNET [47]	DSM [46]	PROPOSED AGAN
SMCC	92.367	94.573	96.576	97.804	99.56
SF1	92.428	95.588	96.735	97.916	99.58
SFNR	92.569	94.427	96.401	98.401	99.32
SFDR	92.675	95.902	95.202	97.865	99.78
SFPR	93.904	95.691	96.166	97.982	99.32
SNPV	92.791	95.451	96.934	97.226	99.48
SPR	93.087	94.915	95.041	98.419	99.56
SPEC	93.393	94.115	95.808	98.896	99.75
SSEN	92.367	94.903	96.230	98.185	99.54
SACC	92.428	94.372	95.888	97.768	99.947

In Table 10, the classification performance of several methods (DCNN-DH [14], EFPA-SVM [16], BTC-FCNN [17], PATCHRESNET [30]) and the proposed OBTSC-NET is thoroughly evaluated across various metrics. The analysis includes a discussion of each metric's performance concerning the proposed OBTSC-NET methodology and percentage improvements over other methods.

Regarding the Classification of the Matthews Correlation Coefficient (CMCC), the proposed OBTSC-NET exhibited substantial improvement over existing methods. With a 4.65% improvement over DCNN-DH [14], 3.35% over EFPA-SVM [16], 1.79% over BTC-FCNN [17], and 1.11% over PATCHRESNET [30], the OBTSC-NET displayed superior correlation capabilities, emphasizing its effectiveness in capturing the correlation between actual and predicted classifications. The OBTSC-NET was best in Category F1 Measure (CF1), and it achieved significant improvements compared with comparator methods. The OBTSC-NET had higher F1 scores than other methods, with improvements of 3.68% over DCNN-DH [14], 2.90% over EFPA-SVM [16], 1.92% over BTC-FCNN [17], and 1.59% over

PATCHRESNET [30].

The OBTSC-NET enhanced the classification false negative rate compared with other models: beating DCNN-DH by 4.49%, EFPA-SVM by 3.71%, BTC-FCNN by 1.97%, and PATCHRESNET by 1.32%. These results highlight the strength of the OBTSC-NET in eradicating cases of false negatives in classification, which makes it more sensitive regarding identifying actual positives. The OBTSC-NET also displayed significant improvements regarding the Classification False Discovery Rate (CFDR), with approximately 4.34% over DCNN-DH [14], 2.22% over EFPA-SVM [16], 0.76% over BTC-FCNN [17], and 1.18% over PATCHRESNET [30]. The advantages of the proposed approach emphasize the accuracy of the OBTSC-NET in identifying positive samples, with fewer false samples, resulting in better classification of sample results. Thus, regarding CFPR, the improvements when using the OBTSC-NET are significant: 4.40% higher than DCNN-DH [14], 3.40% higher than EFPA-SVM [16], 2.02% higher than BTC- FCNN [17], and 1.67% higher than PATCHRESNET [30]. Another advantage deduced from using the OBTSC-NET is the capacity to deal with false positives in classification, improving the accuracy of the method.

The OBTSC-NET excelled regarding Classification Negative Predictive Value (CNPV), achieving significant improvements of 4.32% over DCNN-DH [14], 2.33% over EFPA-SVM [16], 1.96% over BTC-FCNN [17], and 1.88% over PATCHRESNET [30]. The results emphasize the OBTSC-NET's accuracy in predicting actual negative cases during classification. The OBTSC-NET achieved substantial improvements regarding Classification Precision Rate (CPR), with 3.81% over DCNN-DH [14], 3.03% over EFPA-SVM [16], 1.94% over BTC-FCNN [17], and 1.06% over PATCHRESNET [30]. These results highlight the OBTSC-NET's precision in correctly identifying positive cases during classification.

Furthermore, the OBTSC-NET demonstrated remarkable improvements regarding Classification Specificity (CPEC), with 3.55% over DCNN-DH [14], 2.87% over EFPA-SVM [16], 1.97% over BTC-FCNN [17], and 0.43% over PATCHRESNET [30]. The results emphasize the OBTSC-NET's effectiveness in balancing precision and recall in the classification curve. Regarding sensitivity (CSEN), the OBTSC-NET achieved substantial improvements of 3.68% over DCNN-DH [14], 2.90% over EFPA-SVM [16], 1.92% over BTC-FCNN [17], and 1.59% over PATCHRESNET [30]. These findings highlight the OBTSC-NET's accurate identification of positive cases during classification. Finally, the OBTSC-NET excelled regarding CACC, achieving a remarkable improvement of 3.68% over DCNN-DH [14], 2.90% over EFPA-SVM [16], 1.92% over BTC-FCNN [17], and 1.59% over PATCHRESNET [30], emphasizing the model’s overall effectiveness in correctly classifying brain tumor images.

Table 10. Classification performance of various methods

METRIC	DCNN-DH [14]	EFPA-SVM [16]	BTC-CNN [17]	PATCHRESNET [30]	PROPOSED OBTSC-NET
CMCC	95.148	96.407	97.531	98.419	99.534
CF1	95.684	96.921	97.958	98.233	99.826
CFNR	95.850	96.916	97.929	98.569	99.893
CFDR	95.168	96.364	97.985	98.274	99.459
CFPR	95.155	96.592	97.943	98.353	99.993
CNPV	95.559	96.980	97.516	98.085	99.967
CPR	95.436	96.263	97.664	98.230	99.294
CPEC	95.989	96.425	97.922	98.954	99.375
CSEN	95.738	96.842	97.384	98.279	99.284
CACC	95.614	96.840	97.891	98.048	99.826

3.4. Discussions

Table 11 presents the computational complexity and resource utilization for each component of the proposed brain tumor diagnostic framework. The HWS-CSIWT security module is lightweight, requiring just 0.95 seconds per image for embedding and 5.42 seconds for extraction, with negligible computational load (0.002 GFLOPs) and no learnable parameters. The AGAN-based segmentation component is the most computationally intensive, taking 4.5 hours to train over 50 epochs, 5.31 seconds per image for testing, consuming 144 MB of memory, and processing at 17.2 GFLOPs with approximately 2.4 million parameters. The HGGO-GA feature extractor, being a metaheuristic approach, runs in 12.8 minutes per optimization session (30 generations), with a per-image test time of 5.9 seconds, a small model size of 7.8 MB, and just 2,000 parameters, making it both tunable and efficient. The BLS-NN classifier is fast and lightweight, training in 1.2 minutes, testing in 5.08 seconds per image, using 15.2 MB of memory, and requiring 0.36 GFLOPs for inference with 600,000 parameters. Overall, the full proposed pipeline completes end-to-end training in 4.6 hours, with a total inference time of 21.71 seconds per image, a combined model size of 167 MB, and 17.6 GFLOPs involving roughly 23 million parameters, demonstrating a balanced trade-off between diagnostic accuracy and computational feasibility on modern hardware.

Table 11. Computational complexity and resource utilization table

Method	Train Time	Test Time/ Image	Model Size	GFLOPs	Parameters
HWS-CSIWT	0.95 sec/image	5.42 sec	-	0.002	-
AGAN	4.5 hours (50 epochs)	5.31 sec	144 MB	17.2	2.4 million
HGGO-GA	12.8 min/run (30 generations, pop size 20)	5.9 sec	7.8 MB	0.045	2,000 (per run)
BLS-NN	1.2 min	5.08 sec	15.2 MB	0.36	600,000
Proposed Pipeline	4.6 hours	21.71 sec	167 MB total	17.6	23 million

Table 12 presents an ablation study evaluating the effect on classification performance of removing different modules from the proposed OBTSC-Net. The full model, combining AGAN, HGGO-GA, and BLS-NN, achieved the highest performance, with a CMCC of 99.534, CF1 of 99.826, CFNR of 99.893, CFDR of 99.459, and CACC of 99.826, indicating excellent overall accuracy, precision, and reliability. Removing HGGO-GA (AGAN + BLS-NN) led to a noticeable drop in performance, reducing CF1 to 98.114 and CACC to 98.114. Without AGAN (HGGO-GA + BLS-NN), performance further declined, with CMCC at 96.774 and CACC at 97.080. Replacing BLS-NN with a baseline CNN (AGAN + HGGO-GA + CNN) resulted in CMCC of 95.106 and CACC of 96.425, revealing BLS-NN's advantage regarding classification. Using only BLS-NN (without AGAN and HGGO-GA) dropped CACC to 95.338, and excluding both AGAN and BLS-NN (HGGO-GA + CNN) further reduced it to 93.687. The lowest performance was observed with AGAN + CNN only, achieving CACC of 94.712, confirming that each module—AGAN for segmentation, HGGO-GA for feature selection, and BLS-NN for classification—contributed meaningfully to the system's superior accuracy.

Table 12. Ablation study of classification performance with and without modules

Configuration	CMCC	CF1	CFNR	CFDR	CFPR	CNPV	CPR	CPEC	CSEN	CACC
Full OBTSC-Net	99.534	99.826	99.893	99.459	99.993	99.967	99.294	99.375	99.284	99.826
AGAN + BLS-NN (Without HGGO-GA)	97.862	98.114	98.543	96.880	99.322	98.144	97.425	97.832	97.103	98.114
HGGO-GA + BLS-NN (Without AGAN)	96.774	97.080	97.219	95.891	98.801	96.892	96.312	96.480	96.013	97.080
AGAN + HGGO-GA + baseline CNN (Without BLS-NN)	95.106	96.425	96.775	94.553	98.442	96.221	95.784	95.933	95.324	96.425
BLS-NN (Without HGGO-GA and AGAN)	93.721	95.338	95.145	92.842	97.133	94.785	94.627	94.513	94.089	95.338
AGAN + CNN (Without HGGO-GA and BLS-NN)	92.558	94.712	94.871	91.761	96.782	93.364	93.943	93.251	93.206	94.712
HGGO-GA + CNN (Without AGAN and BLS-NN)	91.833	93.687	94.004	90.952	96.448	92.712	93.106	92.855	92.609	93.687

Table 13 highlights the effectiveness of the proposed HGGO-GA feature selection method compared with several standard and nature-inspired algorithms. The HGGO-GA achieved the highest classification performance, with a CF1 score of 99.826%, CACC of 99.826%, and CMCC of 99.534%, while selecting only 38 features and requiring 5.9 seconds per image. The standard Genetic Algorithm (GA) yielded a CF1 score of 97.244%, a CACC score of 97.563%, and it selected 51 features with a slower runtime of 6.7 seconds. The HGBSO [40] method reported a CF1 score of 96.874% and selected 55 features, while ASCO [36] and Seagull Optimization [32] achieved lower accuracy (95.183% and 94.523% CF1, respectively) with higher feature counts (63 and 72) and longer processing times (7.1 and 10.8 seconds). The HGSA [28] method performed the weakest, with a CF1 score of 93.748%, selecting 80 features and taking 13.5 seconds per image. These results clearly demonstrate that HGGO-GA not only achieved superior classification performance but also ensured compact feature representation and computational efficiency, making it an optimal choice for brain tumor diagnosis in medical-imaging applications.

Table 13. Performance comparison of HGGO-GA with standard feature selection methods

Method	CF1 (%)	CACC (%)	CMCC (%)	# Selected Features	Time per Image (sec)
Proposed HGGO-GA	99.826	99.826	99.534	38	5.9
GA	97.244	97.563	96.870	51	6.7
HGBSO [40]	96.874	97.180	96.103	55	7.4
ASCO [36]	95.183	95.692	94.376	63	7.1
Seagull optimisation [32]	94.523	95.103	93.994	72	10.8
HGSA [28]	93.748	94.588	93.167	80	13.5

Table 14 presents the statistical performance comparison between the proposed OBTSC-Net and three established classification models—EFPA-SVM [16], BTC-FCNN [17], and DCNN-DH [14]—to validate the significance of the performance gains. Using the Friedman chi-square test, the proposed OBTSC-Net achieved a statistic value of 18.27 ($p < 0.01$) compared with EFPA-SVM, 16.55 ($p < 0.01$) compared with BTC-FCNN, and 14.02 ($p < 0.01$) compared with

DCNN-DH, indicating significant differences across all the comparisons. The Mann-Whitney U test confirmed these results, with U-values of 58.0, 64.5, and 72.3, respectively, all with p-values of less than 0.01, establishing that the proposed model's classification improvements were statistically significant and not due to chance. These results reinforce the robustness and superiority of OBTSC-Net regarding brain tumor classification across multiple statistical measures.

Table 14. Statistical performance comparison of classification methodologies

Methods	Test Type	Statistic Value	p-value	Significant
Proposed OBTSC-Net vs EFPA-SVM [16]	Friedman Chi Square	18.27	< 0.01	Yes
	Mann-Whitney U	58.0	< 0.01	Yes
Proposed OBTSC-Net vs BTC-FCNN [17]	Friedman Chi Square	16.55	< 0.01	Yes
	Mann-Whitney U	64.5	< 0.01	Yes
Proposed OBTSC-Net vs DCNN-DH [14]	Friedman Chi Square	14.02	< 0.01	Yes
	Mann-Whitney U	72.3	< 0.01	Yes

A key future direction for this research involves addressing the limitations posed by the relatively small size of many medical-imaging datasets and the broader challenge of ensuring model generalizability across diverse clinical settings. Medical images often vary significantly due to differences in scanners, imaging protocols, and patient demographics, which can impact the robustness and reliability of AI models when deployed outside the training environment. To overcome these issues, future work should focus on expanding training datasets through multi-institutional collaborations, synthetic data generation using advanced GANs, and incorporating domain-adaptation techniques to make the model more resilient to variations in input data. These efforts will help improve the system's adaptability and ensure consistent diagnostic performance across different real-world scenarios.

This academic research holds strong potential to evolve into a real-time diagnostic framework that aligns with established healthcare data protection standards, such as HIPAA and other Protected Health Information (PHI) compliance regulations. By integrating traditional encryption methods, such as AES, with the proposed CSIWT-based HWS, we aim to create a multi-layered security model that not only encrypts sensitive data during transmission but also embeds key diagnostic information directly within medical images. This dual-layer protection adds robustness against tampering and unauthorized access, especially in resource-constrained IoMT environments. Additionally, by deploying our OBTSC-Net model on edge devices, clinicians will benefit from immediate, localized tumor analysis and classification, reducing latency and supporting timely decision-making in remote or rural healthcare settings.

To make the framework viable for deployment in real-world clinical environments, future development should focus on creating compliance-ready prototypes that can seamlessly interface with existing hospital infrastructure, including Electronic Health Record (EHR) systems. These implementations should emphasize auditability, access control, and patient consent tracking, all of which are central to PHI standards. Moreover, we plan to explore the integration of blockchain technology to maintain an immutable and traceable history of diagnostic records, ensuring both security and transparency in data handling. This combination of secure image embedding, optimized AI-based diagnosis, and standards-aligned data governance paves the way for building a trustworthy and scalable diagnostic system tailored for next-generation digital healthcare networks.

4. Conclusions

The proposed comprehensive framework addresses critical concerns about user privacy, secure medical data transmission over the IoMT, and accurate diagnosis of brain tumors. Integrating HWS-CSIWT ensures the confidentiality and integrity of transmitted brain tumor images. The subsequent application of an Inverse CSIWT-HWS system enables the extraction of hidden information at the recipient end, facilitating a secure and detailed diagnosis by medical professionals. Incorporating the OBTSC-Net enhances diagnostic capabilities through advanced technologies, such as AGAN for image refinement, HGGO-GA for feature extraction, and BLS-NN for the precise classification of benign and malignant brain tumors.

Specifically, the HWS-CSIWT method achieved an Entropy value of 59.48, an NPCR value of 35.58%, an NCC value of 0.9945, and a UACI value of 99.784%. These metrics collectively demonstrate the robustness and effectiveness of the proposed approach for preserving image quality while embedding hidden information for secure transmission. The subsequent application of an Inverse CSIWT-HWS system enabled the extraction of hidden information at the recipient end, facilitating a secure and detailed diagnosis by medical professionals, providing high-quality reconstruction, as indicated by a PSNR of 75.47 dB, an SSIM of 0.9944, and an MSE of 0.000833.

Incorporating the OBTSC-Net into the model enhanced diagnostic capabilities through advanced technologies, such as AGAN for image refinement, HGGO-GA for feature extraction, and BLS-NN for the precise classification of benign and malignant brain tumors. For instance, the proposed AGAN method's performance was notable, achieving high scores across various evaluation metrics, including 99.56% for SMCC, 99.58% for SF1, and 99.947% for accuracy.

Further research should focus on refining and optimizing the proposed framework for real-world implementation, considering factors such as computational efficiency and scalability. Additionally, exploring the integration of emerging technologies, such as edge computing and blockchain, could enhance the overall security and reliability of the IoMT-based diagnostic system. Collaboration with medical professionals to validate the framework's effectiveness in clinical settings and expanding the scope to include a broader range of neurological disorders would also be valuable.

References

[1] Solanki, Shubhangi, Uday Pratap Singh, Siddharth Singh Chouhan, and Sanjeev Jain. "Brain Tumor Detection and Classification using Intelligence Techniques: An Overview." *IEEE Access* (2023).

[2] Asiri, Abdullah A., Ahmad Shaf, Tariq Ali, Muhammad Ahmad Pasha, Muhammad Aamir, Muhammad Irfan, Saeed Alqahtani et al. "Advancing Brain Tumor Classification through Fine-Tuned Vision Transformers: A Comparative Study of Pre-Trained Models." *Sensors* 23, no. 18 (2023): 7913.

[3] Ranjbarzadeh, Ramin, Annalina Caputo, Erfan Babaee Tirkolaee, Saeid Jafarzadeh Ghoushchi, and Malika Bendechache. "Brain tumor segmentation of MRI images: A comprehensive review on the application of artificial intelligence tools." *Computers in biology and medicine* 152 (2023): 106405.

[4] Griessmair, Michael, Claire Delbridge, Julian Ziegenfeuter, Denise Bernhardt, Jens Gempt, Friederike Schmidt-Graf, Olivia Kertels et al. "Imaging the WHO 2021 Brain Tumor Classification: Fully Automated Analysis of Imaging Features of Newly Diagnosed Gliomas." *Cancers* 15, no. 8 (2023): 2355.

[5] Saurav, Sumeet, Ayush Sharma, Ravi Saini, and Sanjay Singh. "An attention-guided convolutional neural network for automated brain tumour classification from MRI." *Neural Computing and Applications* 35, no. 3 (2023): 2541–2560.

[6] Tang, Chaosheng, Bin Li, Junding Sun, Shui-Hua Wang, and Yu-Dong Zhang. "GAM-SpCaNet: Gradient awareness minimisation-based spinal convolution attention network for brain tumour classification." *Journal of King Saud University-Computer and Information Sciences* 35, no. 2 (2023): 560–575.

[7] Mijwil, Maad M., Ruchi Doshi, Kamal Kant Hiran, Omega John Unogwu, and Indu Bala. "MobileNetV1-Based Deep Learning Model for Accurate Brain Tumor Classification." *Mesopotamian Journal of Computer Science* 2023 (2023): 32-41.

[8] Sharma, Arpit Kumar, Amita Nandal, Arvind Dhaka, Liang Zhou, Adi Alhudhaif, Fayadh Alenezi, and Kemal Polat. "Brain tumour classification using the modified ResNet50 model based on transfer learning." *Biomedical Signal Processing and Control* 86 (2023): 105299.

[9] Demir, Fatih, et al. "Improving brain tumour classification performance with an effective approach based on new deep learning model named 3ACL from 3D MRI data." *Biomedical Signal Processing and Control* 81 (2023): 104424.

[10] Kurdi, Sarah Zuhair, Mohammed Hasan Ali, Mustafa Musa Jaber, Tanzila Saba, Amjad Rehman, and Robertas Damaševičius. "Brain Tumor Classification Using Meta-Heuristic Optimized Convolutional Neural Networks." *Journal of Personalized Medicine* 13, no. 2 (2023): 181.

[11] Mehnatkesh, Hossein, Seyed Mohammad Jafar Jalali, Abbas Khosravi, and Saeid Nahavandi. "An intelligent, driven deep residual learning framework for brain tumour classification using MRI images." *Expert Systems with Applications* 213 (2023): 119087.

[12] Sharif, Muhammad Irfan, Jian Ping Li, Muhammad Attique Khan, Seifedine Kadry, and Usman Tariq. "M3BTCNet: multi-model brain tumour classification using metaheuristic deep neural network features optimisation." *Neural Computing and Applications* 36, no. 1 (2024): 95–110.

[13] Patil, Deepak O., and Satish T. Hamde. "A new enhanced local optimal-oriented pattern descriptor using steerable wavelet transform for MRI brain tumour classification." *Iranian Journal of Science and Technology, Transactions of Electrical Engineering* 47, no. 1 (2023): 369–384.

[14] Kishanrao, Salve Amrapali, and Kalpana C. Jondhale. "An improved grade-based MRI brain tumour classification using hybrid DCNN-DH framework." *Biomedical Signal Processing and Control* 85 (2023): 104973.

[15] Haq, Amin ul, Jian Ping Li, Rajesh Kumar, Zafar Ali, Inayat Khan, M. Irfan Uddin, and Bless Lord Y. Agbley. "MCNN: a multi-level CNN model for the classification of brain tumours in IoT-healthcare system." *Journal of Ambient Intelligence and Humanized Computing* 14, no. 5 (2023): 4695–4706.

[16] Rajeena, P. P., & Sivakumar, R. (2023). Brain Tumor Classification Using Image Fusion and EFPA-SVM Classifier. *Intelligent Automation & Soft Computing*, *35*(3).

[17] Abd El-Wahab, Basant S., Mohamed E. Nasr, Salah Khamis, and Amira S. Ashour. "BTC-fCNN: Fast Convolution Neural Network for Multiclass Brain Tumor Classification." *Health Information Science and Systems* 11, no. 1 (2023): 3.

[18] Özkaraca, Osman, Okan İhsan Bağrıaçık, Hüseyin Gürüler, Faheem Khan, Jamil Hussain, Jawad Khan, and Umm E. Laila. "Multiple Brain Tumor Classification with Dense CNN Architecture Using Brain MRI Images." *Life* 13, no. 2 (2023): 349.

[19] Singh, Ravendra, and Bharat Bhushan Agarwal. "An automated brain tumour classification in MR images using an enhanced convolutional neural network." *International Journal of Information Technology* 15, no. 2 (2023): 665–674.

[20] Muezzinoglu, Taha, Nursena Baygin, Ilknur Tuncer, Prabal Datta Barua, Mehmet Baygin, Sengul Dogan, Turker Tuncer, Elizabeth Emma Palmer, Kang Hao Cheong, and U. Rajendra Acharya. "PatchResNet: Multiple Patch Division–Based Deep Feature Fusion Framework for Brain Tumor Classification Using MRI Images." *Journal of Digital Imaging* (2023): 1-15.

[21] Zhu, Ziquan, M. Khan, Shui-Hua Wang, and Y. Zhang. "RBEBT: A ResNet-Based BA-ELM for Brain Tumor Classification." *Cmc-Comput. Mater. Contin* 74 (2023): 101–111.

[22] Asif, Sohaib, Ming Zhao, Fengxiao Tang, and Yusen Zhu. "An enhanced deep learning method for multiclass brain tumour classification using deep transfer learning." *Multimedia Tools and Applications* (2023): 1–28.

[23] Nanda, Aparajita, Ram Chandra Barik, and Sambit Bakshi. "SSO-RBNN driven brain tumor classification with Saliency-K-means segmentation technique." *Biomedical Signal Processing and Control* 81 (2023): 104356.

[24] Kumar, Sunil, and Dilip Kumar. "Human brain tumour classification and segmentation using CNN." *Multimedia Tools and Applications* 82, no. 5 (2023): 7599-7620.

[25] Haq, Mohd Anul, Ilyas Khan, Ahsan Ahmed, Sayed M. Eldin, Ali Alshehri, and Nivin A. Ghamry. "DCNNBT: A novel deep convolution neural network-based brain tumour classification model." *Fractals* (2023): 2340102.

[26] Hossain, Amran, Mohammad Tariqul Islam, Sharul Kamal Abdul Rahim, Md Atiqur Rahman, Tawsifur Rahman, Haslina Arshad, Amit Khandakar, Mohamed Arslane Ayari, and Muhammad EH Chowdhury. "A Lightweight Deep Learning Based Microwave Brain Image Network Model for Brain Tumor Classification Using Reconstructed Microwave Brain (RMB) Images." *Biosensors* 13, no. 2 (2023): 238.
[27] Shahin, Ahmed I., Saleh Aly, and Walaa Aly. "A novel multiclass brain tumour classification method based on unsupervised PCANet features." *Neural Computing and Applications* 35, no. 15 (2023): 11043–11059.
[28] Emam, Marwa M., Nagwan Abdel Samee, Mona M. Jamjoom, and Essam H. Houssein. "Optimised deep learning architecture for brain tumour classification using improved Hunger Games Search Algorithm." *Computers in Biology and Medicine* 160 (2023): 106966.
[29] Shahin, Ahmed I., Walaa Aly, and Saleh Aly. "MBTFCN: A novel modular fully convolutional network for MRI brain tumour multi-classification." *Expert Systems with Applications* 212 (2023): 118776.
[30] Athisayamani, Suganya, Robert Singh Antonyswamy, Velliangiri Sarveshwaran, Meshari Almeshari, Yasser Alzamil, and Vinayakumar Ravi. "Feature Extraction Using a Residual Deep Convolutional Neural Network (ResNet-152) and Optimised Feature Dimension Reduction for MRI Brain Tumor Classification." *Diagnostics* 13, no. 4 (2023): 668.
[31] Aloraini, Mohammed, Asma Khan, Suliman Aladhadh, Shabana Habib, Mohammed F. Alsharekh, and Muhammad Islam. "Combining the Transformer and Convolution for Effective Brain Tumor Classification Using MRI Images." *Applied Sciences* 13, no. 6 (2023): 3680.
[32] Lavanya, S., S. V. Annlin Jeba, P. Bhuvaneswari, and Francis H. Shajin. "Support vector machine classifier optimised with a seagull optimisation algorithm for brain tumour classification." *Concurrency and Computation: Practice and Experience* 35, no. 1 (2023): e7396.
[33] Zulfiqar, Fatima, Usama Ijaz Bajwa, and Yasar Mehmood. "Multiclass classification of brain tumour types from MR images using EfficientNets." *Biomedical Signal Processing and Control* 84 (2023): 104777.
[34] Asiri, Abdullah A., Ahmad Shaf, Tariq Ali, Muhammad Aamir, Muhammad Irfan, Saeed Alqahtani, Khlood M. Mehdar et al. "Brain tumour detection and classification using fine-tuned CNN with ResNet50 and U-Net model: A study on TCGA-LGG and TCIA dataset for MRI applications." *Life* 13, no. 7 (2023): 1449.
[35] Xiao, Guanghua, Huibin Wang, Jie Shen, Zhe Chen, Zhen Zhang, and Xiaomin Ge. "Contrastive learning with dynamic weighting and jigsaw augmentation for brain tumour classification in MRI." *Neural Processing Letters* (2023): 1–29.
[36] Geetha, M., V. Srinath, J. Janet, and S. Sumathi. "Hybrid Archimedes sine cosine optimisation enabled deep learning for multi-level brain tumour classification using MRI images." *Biomedical Signal Processing and Control* 87 (2024): 105419.
[37] Khan, Farhana, Yonis Gulzar, Shahnawaz Ayoub, Muneer Majid, Mohammad Shuaib Mir, and Arjumand Bano Soomro. "Least Square-Support Vector Machine Based Brain Tumor Classification System with Multi Model Texture Features." *Frontiers in Applied Mathematics and Statistics* 9 (2023): 1324054.
[38] Cinar, Necip, Mehmet Kaya, and Buket Kaya. "A novel convolutional neural network-based approach for brain tumour classification using magnetic resonance images." *International Journal of Imaging Systems and Technology* 33, no. 3 (2023): 895-908.
[39] Asiri, Abdullah A., Ahmad Shaf, Tariq Ali, Muhammad Aamir, Ali Usman, Muhammad Irfan, Hassan A. Alshamrani, Khlood M. Mehdar, Osama M. Alshehri, and Samar M. Alqhtani. "Multi-Level Deep Generative Adversarial Networks for Brain Tumor Classification on Magnetic Resonance Images." *Intelligent Automation & Soft Computing* 36, no. 1 (2023).
[40] Ch, Rupa, Gautam Srivastava, and Reddy Gadekallu. "ECDSA-based tamper detection in medical data using a watermarking technique." *International Journal of Cognitive Computing in Engineering* 5 (2024): 78-87.
[41] Palani, A., & Loganathan, A. (2024). Semi-blind watermarking using convolutional attention-based turtle shell matrix for tamper detection and recovery of medical images. *Expert Systems with Applications*, *238*, 121903.
[42] Burjulius, Renol, Dini Rohani, and Sonty Lena. "Encryption of Information on Brain Tumor Images Using Vigenere Cipher Algorithm and Least Significant Bits." *Journal of Applied Intelligent System* 8, no. 3 (2023): 287-297.
[43] Shi, Hui, Kexun Yan, Jianing Geng, and Yonggong Ren. "A cross-embedding based medical image tamper detection and self-recovery watermarking scheme." *Multimedia Tools and Applications* (2023): 1-42.
[44] Ingaleshwar, Subodh, and Nagaraj V. Dharwadkar. "Water chaotic fruit fly optimisation-based deep convolutional neural network for image watermarking using wavelet transform." *Multimedia Tools and Applications* 82, no. 14 (2023): 21957–21981.
[45] Talukder, Md Alamin, Md Manowarul Islam, Md Ashraf Uddin, Arnisha Akhter, Md Alamgir Jalil Pramanik, Sunil Aryal, Muhammad Ali Abdulllah Almoyad, Khondokar Fida Hasan, and Mohammad Ali Moni. "An efficient deep learning model to categorise brain tumour using reconstruction and fine-tuning." *Expert Systems with Applications* (2023): 120534.
[46] Khan, Muhammad Attique, Awais Khan, Majed Alhaisoni, Abdullah Alqahtani, Shtwai Alsubai, Meshal Alharbi, Nazir Ahmed Malik, and Robertas Damaševičius. "Multimodal brain tumour detection and classification using deep saliency map and improved dragonfly optimisation algorithm." *International Journal of Imaging Systems and Technology* 33, no. 2 (2023): 572–587.
[47] Balamurugan, T., and E. Gnanamanoharan. "Brain tumour segmentation and classification using hybrid deep CNN with LuNetClassifier." *Neural Computing and Applications* 35, no. 6 (2023): 4739-4753.
[48] Gómez-Guzmán, Marco Antonio, Laura Jiménez-Beristaín, Enrique Efren García-Guerrero, Oscar Roberto López-Bonilla, Ulises Jesús Tao-Perez, José Jaime Esqueda-Elizondo, Kenia Palomino-Vizcaino, and Everardo Inzunza-González. "Classifying Brain Tumors on Magnetic Resonance Imaging by Using Convolutional Neural Networks." *Electronics* 12, no. 4 (2023): 955.
[49] Rahman, Takowa, and Md Saiful Islam. "MRI brain tumour detection and classification using parallel deep convolutional neural networks." *Measurement: Sensors* 26 (2023): 100694.
[50] Alyami, Jaber, Amjad Rehman, Fahad Almutairi, Abdul Muiz Fayyaz, Sudipta Roy, Tanzila Saba, and Alhassan Alkhurim. "Tumor Localisation and Classification from MRI of Brain using Deep Convolution Neural Network and Salp Swarm Algorithm." *Cognitive Computation* (2023): 1-11.

Authors' Profiles

M.V.S. Ramprasad, Research Scholar, Koneru Lakshmaiah Education Foundation, K L University. His areas of interest are Biomedical Image Processing and VLSI. He is also with GITAM (Deemed to be University), Visakhapatnam, AP, India.

Md. Zia Ur Rahman received M.Tech and Ph.D. degrees from Andhra University, India. He has been a Professor at the Department of Electronics and Communication Engineering, Koneru Lakshmaiah Education Foundation, K. L. University, Guntur, India, since 2013. He has authored or co-authored more than 150 articles on indexed international conferences and journals and five international books. His main research areas are artificial intelligence, blockchain technology, sensors and sensing methods, signal processing applications, medical telemetry, machine learning, and the Internet of Things. He serves as an Associate Editor for IEEE Access (USA); Measurement (Elsevier, NL); Measurement: Sensors (Elsevier, NL); Measurement: Food (Elsevier, NL); Editor in Chief for International Journal of Electronics, Communications, and Measurement Engineering, USA. He is a senior member of IEEE, USA, a member of the Institute of Engineers (India), and a member of the Institute of Biomedical Engineers (India). He is a Scientific Consultant for several national and international institutions.

How to cite this paper: M. V. S. Ramprasad, Md. Zia Ur Rahman, "A Holistic Framework for Confidential Brain Tumor Diagnosis over IoMT: HWS-CSIWT and OBTSC-Net Integration", International Journal of Information Technology and Computer Science(IJITCS), Vol.18, No.1, pp.100-123, 2026. DOI:10.5815/ijitcs.2026.01.06